International Journal of Solids and Structures 50 (2013) 773–780

Contents lists available at SciVerse ScienceDirect

International Journal of Solids and Structures

journal homepage: www.elsevier.com/locate/ijsolstr

Modifications of the Newton–Raphson method for finite element simulations in ferroelectroelasticity

S. Stark [a,*], S. Roth [b], P. Neumeister [a], H. Balke [a]

[a] Institute of Solid Mechanics, Technische Universität Dresden, Mommsenstraße 13, 01062 Dresden, Germany
[b] Institute of Mechanics and Fluid Dynamics, Technische Universität Bergakademie Freiberg, Lampadiusstraße 4, 09599 Freiberg, Germany

ARTICLE INFO

Article history:
Received 10 September 2012
Received in revised form 8 November 2012
Available online 25 November 2012

Keywords:
Algorithms
Diverging
Finite element
Ferroelectroelasticity
Scalar potential

ABSTRACT

The system of equations arising in finite element simulations of components made of ferroelectroelastic materials is non-linear if the loading is sufficiently high. The Newton–Raphson method represents a widely used iterative technique to solve this system of non-linear equations. However, if the scalar potential formulation is utilised, convergence difficulties may occur. This circumstance can be primarily attributed to the specific form of the non-linear response of typical ferroelectroelastic materials being subjected to electrical loading. The present paper is devoted to modifications of the Newton–Raphson method, which are capable of improving the convergence behaviour experienced in the finite element iteration. We extend an existing modification to the fully coupled, ferroelectroelastic case. Additionally, a new modification of the Newton–Raphson method is proposed. This method applies an iteration algorithm, which is virtually equivalent to the iteration algorithm of the unmodified Newton–Raphson method combined with the vector potential formulation. An important feature of both modifications is that they are applied on the integration point level. Therefore, the global non-linear finite element iteration scheme remains unchanged. Finally, the practicability of the modifications discussed in the paper is shown in a numerical example.

1. Introduction

Polycrystalline ferroelectroelastic ceramics are used for actuator and sensor applications due to their outstanding piezoelectric properties. However, a process called "poling" is necessary to induce these properties. During poling, a high electric field is applied, which leads to the development of a macroscopic remanent polarisation and strain. In a similar fashion, mechanical or combined electrical and mechanical loading can cause a change in remanence as well.

Macroscopic and microscopic material models describing the irreversible material behaviour of ferroelectroelastic ceramics have been developed by several authors (e.g. Cocks and McMeeking, 1999; Landis, 2002a; Kamlah and Wang, 2003; Mehling et al., 2007; Klinkel, 2006; Huo and Jiang, 1997; Hwang et al., 1995; Huber et al., 1999; Pathak and McMeeking, 2008; Neumeister and Balke, 2011, respectively). In the following, we restrict ourselves to the isothermal and rate-independent class of phenomenological, macroscopic material models (Cocks and McMeeking, 1999; Landis, 2002a; Kamlah and Wang, 2003; Mehling et al., 2007; Klinkel, 2006), which assume a single switching surface and purely kinematic hardening. These material models must describe the essential features of the material behaviour observed in experiments during poling. Consequently, all of them have in common that the initially linear dielectric response of a virgin ceramic being subjected to a monotonically increasing electric field is followed by a sudden increase in remanent polarisation. This causes a jump in the apparent permittivity, which can be observed as a "kink" in plots of electric displacement vs. electric field. If the electric field is increased further, saturation of the remanent polarisation occurs and the material behaviour is virtually linear dielectric again. Roth et al. (2009) have shown that this specific material response may give rise to oscillating or diverging solutions during Newton–Raphson iterations in finite element simulations if the scalar potential formulation (Allik and Hughes, 1970) is used. This finding motivates the investigation and development of modified Newton–Raphson methods. However, most of the modified Newton–Raphson methods known from literature are not suitable to avoid the convergence problems. E.g., the use of the initial tangent matrix for all iteration steps leads to similar difficulties as experienced in the unmodified Newton–Raphson method. Also more sophisticated algorithms like the line search method can not guarantee convergence as discussed by Roth et al. (2009). Therefore, these authors present two new modifications of the Newton–Raphson method for the electromechanically uncoupled, purely ferroelectric case. While the so-called "γ-modification" is

* Corresponding author. Tel.: +49 351 463 33285; fax: +49 351 463 32450.
E-mail addresses: Sebastian.Stark1@tu-dresden.de (S. Stark), Stephan.Roth@imfd.tu-freiberg.de (S. Roth), Peter.Neumeister@tu-dresden.de (P. Neumeister), Herbert.Balke@tu-dresden.de (H. Balke).

0020-7683/$ - see front matter © 2012 Elsevier Ltd. All rights reserved.
http://dx.doi.org/10.1016/j.ijsolstr.2012.11.008

based upon a scaling of the local electric displacement residuals at each integration point of the finite elements, the "τ-modification" utilises a scaling of the tangent permittivity. Both modifications require the choice of numerical parameters controlling their convergence properties. Another approach to overcome the described convergence difficulties of the scalar potential formulation is the use of the vector potential formulation proposed by Landis (2002b). However, this formulation has the disadvantage that it requires two additional degrees of freedom per finite element node over the scalar potential formulation for three-dimensional problems. Moreover, gauging is necessary to achieve uniqueness of the vector potential in three dimensions and the application of boundary conditions is not a trivial task in general (Semenov et al., 2006). The last two difficulties can be avoided at the cost of one further degree of freedom per finite element node by using a hybrid finite element formulation (Ghandi and Hagood, 1997; Schwaab et al., 2012).

The present paper focuses on modifications of the Newton–Raphson method, where the scalar potential formulation is used. In the first part, we consider the simulation of the poling process of an electromechanically uncoupled, purely ferroelectric ceramic assuming homogeneous field distributions. The reasons for the convergence difficulties experienced with the unmodified Newton–Raphson method are briefly explained together with the γ-modification, which avoids these difficulties. Additionally, a new modification of the Newton–Raphson method is introduced. This modification will be called "D-modification" in the following. The second part of the paper deals with the generalisation of the γ-modification and the D-modification to the multi-axial, fully coupled, ferroelectroelastic case. In the last part, the poling of a hexahedron containing a centered cylindrical hole is simulated with the finite element method. In this context, the γ-modification and the D-modification of the Newton–Raphson method are compared to their unmodified counterpart and the vector potential formulation.

All tensor equations in this paper are written in co-ordinate notation, with summation implied over repeated indices. Furthermore, we assume cartesian co-ordinates. Therefore, the terms "vector" and "tensor" are used even though only their co-ordinates are addressed.

2. Homogeneous poling of an electromechanically uncoupled, purely ferroelectric ceramic

For a general discussion of the convergence difficulties mentioned above, it is sufficient to consider homogeneous field distributions. Hence, the behaviour of the global Newton–Raphson iteration of a finite element simulation can be studied on the material point level. Furthermore, an electromechanically uncoupled, purely ferroelectric ceramic under electrical loading in a fixed direction is assumed, where the material is free of remanent polarisation initially. Consequently, all mechanical quantities vanish and the state of the material can be characterised with the electric field E and the remanent polarisation P^{r}. Given that E and P^{r} specify an admissible material state, the corresponding electric displacement D can be directly calculated from these quantities.

The starting point for our discussion is a reference state of the material, which is described with the reference electric field E^{ref} and the reference remanent polarisation $P^{\mathrm{r,ref}}$. The associated reference electric displacement is D^{ref}. We assume that the electric displacement is changed monotonically during a single load step from its value $D = D^{\mathrm{ref}}$ in the reference state to $D = D^{\mathrm{ext}}$ by applying additional free charges from an external source on the surface of the body under consideration. It is now the task to determine the electric field E^{ext} corresponding to the loading D^{ext}. If the scalar potential formulation is utilised, the electric field has to be viewed as the independent variable, since it is derived by differentiation from the scalar potential ϕ. Therefore, the relationship between E^{ext} and D^{ext} is given in the form

$$D^{\mathrm{ext}} = D^{\mathrm{mat}}\left(E^{\mathrm{ext}}, P^{\mathrm{r,ref}}, E^{\mathrm{ref}}\right), \tag{1}$$

where the function $D^{\mathrm{mat}}(E, P^{\mathrm{r,ref}}, E^{\mathrm{ref}})$ is used. This function assigns the "material electric displacement" based upon the electric field E at the end of the load step and the parameters $P^{\mathrm{r,ref}}$ and E^{ref} characterising the reference state. Note, that D^{mat} is usually implemented by applying so-called "return mapping" algorithms (see e.g. Semenov et al., 2009). In general, the formulation of such a function requires an (implicit) assumption for the loading path traversed within the load step. However, this loading path is unique for the one dimensional case with monotonic loading considered here. In the following, the parameter E^{ref} in D^{mat} is omitted since the electric field in the reference state is not relevant for typical phenomenological, macroscopic material models.

Due to the fact that the electric displacement D^{ext} at the end of the load step is prescribed here, Eq. (1) has to be solved for E^{ext}. Given an approximation $E^{(k),\mathrm{ext}}$ for the solution of this problem in the kth step of a numerical iteration scheme, a new approximation $E^{(k+1),\mathrm{ext}}$ may be calculated by using the "global" iteration rule

$$E^{(k+1),\mathrm{ext}} = E^{(k),\mathrm{ext}} + \frac{D^{\mathrm{ext}} - D^{(k),\mathrm{int}}}{\kappa^{(k),\mathrm{int}}}. \tag{2}$$

Here, the "internal" electric displacement $D^{(k),\mathrm{int}}$ and the "internal" permittivity $\kappa^{(k),\mathrm{int}}$ depend on the iteration method utilised. These quantities have to be provided by the "local material routines", which are seen as a "black box". Within this black box, $D^{(k),\mathrm{int}}$ and $\kappa^{(k),\mathrm{int}}$ must be chosen suitably to allow for convergence of the numerical iteration scheme to a valid solution. Note, that for the simplified case considered here, Eq. (2) corresponds to a "global equilibrium iteration step" within a non-linear finite element analysis. Since all modifications of the Newton–Raphson method discussed below are applied locally for all material points associated with integration points of the finite elements, the global iteration scheme (here represented by Eq. (2)) is not altered. Note also, that D^{ext} in Eq. (2) need not be constant during the iteration process in general. This is a point we return to below.

2.1. Unmodified Newton–Raphson method

For the unmodified Newton–Raphson method the quantities $D^{(k),\mathrm{int}}$ and $\kappa^{(k),\mathrm{int}}$ in Eq. (2) are determined by

$$D^{(k),\mathrm{int}} = D^{\mathrm{mat}}\left(E^{(k),\mathrm{ext}}, P^{\mathrm{r,ref}}\right), \tag{3}$$

$$\kappa^{(k),\mathrm{int}} = \kappa^{\mathrm{mat}}\left(E^{(k),\mathrm{ext}}, P^{\mathrm{r,ref}}\right), \tag{4}$$

where the consistent tangent permittivity is defined as

$$\kappa^{\mathrm{mat}}\left(E, P^{\mathrm{r,ref}}\right) = \frac{\partial D^{\mathrm{mat}}}{\partial E}. \tag{5}$$

To explain the convergence problems arising in the unmodified Newton–Raphson method, we start from a virgin, unloaded ceramic. Thus, we have $E^{\mathrm{ref}} = 0$, $P^{\mathrm{r,ref}} = 0$ and $D^{\mathrm{ref}} = 0$ in the reference state. The function D^{mat} relevant for an increase of the applied load from $D^{\mathrm{ref}} = 0$ to $D^{\mathrm{ext}} > 0$ is assumed as follows:

$$D^{\mathrm{mat}}\left(E, P^{\mathrm{r,ref}} = 0\right) = P^{\mathrm{r}} + \kappa E, \tag{6}$$

with

$$\frac{P^{\mathrm{r}}}{P_0} = \begin{cases} 0 & E \leqslant E_0, \\ \sqrt{1 - \left(\frac{P_0 - \kappa E}{P_0 - \kappa E_0}\right)^2} & E_0 < E < \frac{P_0}{\kappa}, \\ 1 & E \geqslant \frac{P_0}{\kappa}. \end{cases} \tag{7}$$

Here, κ denotes the linear permittivity, E_0 is the coercive electric field characterising the onset of irreversible material behaviour and P_0 is the remanent saturation polarisation, which is achieved for electric fields $E \geqslant P_0/\kappa$. Furthermore, we require $E_0 < P_0/\kappa$. Note, that Eq. (7) represents an ellipse with respect to P^{r} and E for $E_0 < E < P_0/\kappa$. Note further, that the function D^{mat} specified in (6) and (7) resembles the electric response of typical ferroelectroelastic ceramics during poling from the virgin state at least qualitatively. Now, take e.g. the loading $D^{\mathrm{ext}} = P_0$ and $E^{(0),\mathrm{ext}} = 0$ as initial guess for the unmodified Newton–Raphson iteration. According to Eqs. (3)–(7) this yields $\kappa^{(0),\mathrm{int}} = \kappa$ and $D^{(0),\mathrm{int}} = 0$. Thus, it follows from (2) that $E^{(1),\mathrm{ext}} = P_0/\kappa$. Repeating the procedure gives $\kappa^{(1),\mathrm{int}} = \kappa$, $D^{(1),\mathrm{int}} = 2P_0$ and $E^{(2),\mathrm{ext}} = 0$. Due to the fact that $E^{(2),\mathrm{ext}} = E^{(0),\mathrm{ext}}$, the solution oscillates between $E^{(k),\mathrm{ext}} = 0$ and $E^{(k),\mathrm{ext}} = P_0/\kappa$ in all subsequent iterations. This is visualised in Fig. 1(a) for the case $\kappa E_0/P_0 = 0.2$. The material response characterised by D^{mat} according to Eqs. (6) and (7) is plotted as a thick line in normalised form vs. the electric field. The horizontal dashed line indicates the level of loading $D^{\mathrm{ext}} = P_0$, while the thin chain dotted lines illustrate the oscillating iteration process, which consists of equilibrium iterations and material update (return mapping) steps. A new approximation $E^{(\mathrm{k}+1),\mathrm{ext}}$ is obtained graphically by intersecting the tangent to the curve D^{mat} in the point $E^{(\mathrm{k}),\mathrm{ext}}$ with the dashed line given by the loading D^{ext}. Evidently, the oscillating solutions are caused by the "kink" in the material response signifying the transition between reversible and irreversible material behaviour at $E = E_0$. If this sharp "kink" is slightly smoothened, it becomes clear that it corresponds to an inflection point in the function $D^{\mathrm{mat}}(E, P^{\mathrm{r,ref}} = 0)$, where the curvature is negative beyond $E = E_0$. The fact that the Newton–Raphson method can fail in one dimension if an inflection point is close to the root is well known. However, the convergence behaviour depends on the characteristics of the inflection point (i.e. whether the sign of the curvature changes from negative to positive or from positive to negative as it is the case here). Therefore, it is not surprising that the vector potential formulation, which utilises the electric displacement as an independent variable, does not show the convergence problems of the scalar potential formulation. Note, that the unmodified Newton–Raphson method converges for high loadings $D^{\mathrm{ext}} > P_0 + \kappa E_0$ for the same initial guess as above ($E^{(0),\mathrm{ext}} = 0$).

2.2. γ-Modification of the Newton–Raphson method

For the so-called "γ-modification" developed by Roth et al. (2009) the quantities $D^{(k),\mathrm{int}}$ and $\kappa^{(k),\mathrm{int}}$ in Eq. (2) are determined by

$$D^{(k),\mathrm{int}} = D^{\mathrm{ext}} + \gamma^{(k)}\left[D^{\mathrm{mat}}\left(E^{(k),\mathrm{ext}}, P^{\mathrm{r,ref}}\right) - D^{\mathrm{ext}}\right] = D^{\mathrm{ext}} + \gamma^{(k)}\Delta D^{(k)}, \quad (8)$$

$$\kappa^{(k),\mathrm{int}} = \kappa^{\mathrm{mat}}\left(E^{(k),\mathrm{ext}}, P^{\mathrm{r,ref}}\right), \quad (9)$$

where $0 < \gamma^{(k)} \leqslant 1$ is a parameter scaling the local electric displacement residual $\Delta D^{(k)} = D^{\mathrm{mat}}(E^{(k),\mathrm{ext}}, P^{\mathrm{r,ref}}) - D^{\mathrm{ext}}$ computed after the iteration steps. The empirical relation

$$\gamma^{(k)} = (1 - M) \cdot \exp\left(-\frac{\left|\Delta D^{(k)}\right|}{P_0 L}\right) + M \quad (10)$$

is used for $\gamma^{(k)}$, with $0 \leqslant M \leqslant 1$ and $L > 0$ being numerical parameters (Roth et al., 2009). In order to achieve convergence of the iterative procedure, these parameters have to be chosen appropriately, depending on the material behaviour involved. The γ-modification is identical to the unmodified Newton–Raphson method for $\gamma^{(k)} = 1$ (and therefore $M = 1$). Furthermore, the inequality $\gamma^{(k)} \geqslant M$ always holds. Let $d^{(k)} = |\Delta D^{(k)}|/P_0$ be a measure for the

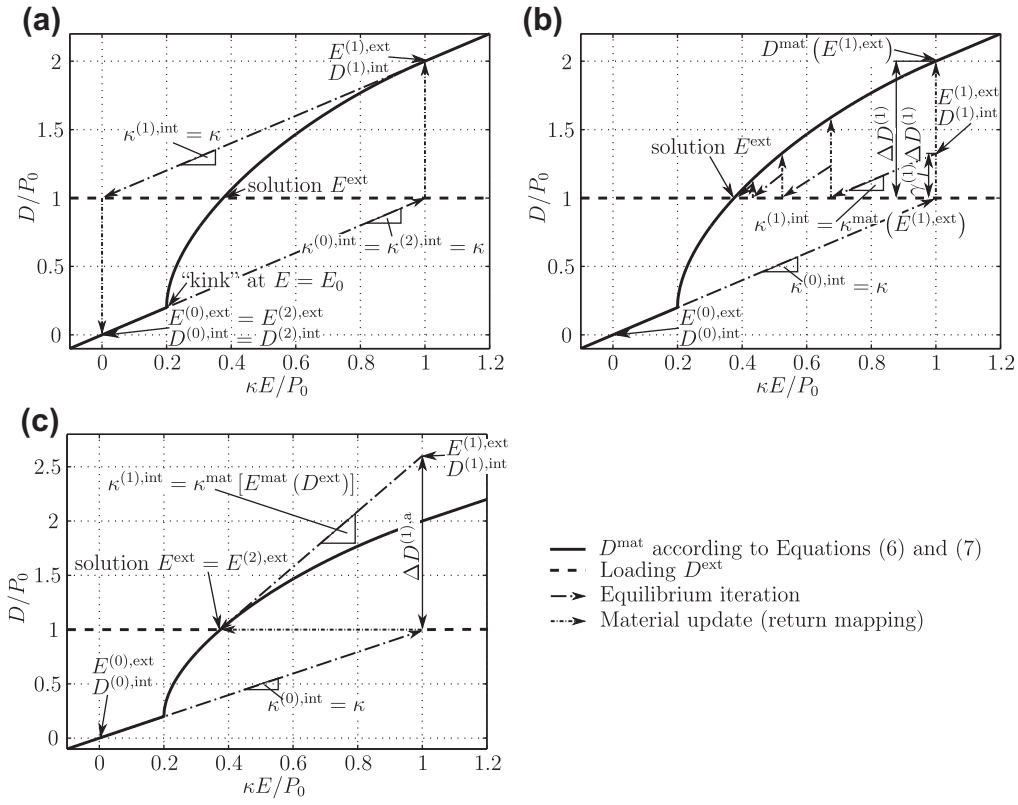

Fig. 1. (a) Unmodified Newton–Raphson method; oscillating iteration procedure for $D^{\mathrm{ext}} = P_0$ and $\kappa E_0/P_0 = 0.2$ (b) γ-modification; converging iteration procedure for $D^{\mathrm{ext}} = P_0$, $\kappa E_0/P_0 = 0.2$, $M = L = 0.3$ (c) D-modification; converging iteration procedure for $D^{\mathrm{ext}} = P_0$, $\kappa E_0/P_0 = 0.2$.

accuracy of the solution obtained after the kth equilibrium iteration and return mapping step. Then, as can be seen from (10), $d^{(k)} \gg L$ leads to $\gamma^{(k)} \approx M$ and $d^{(k)} \ll L$ gives $\gamma^{(k)} \approx 1$. The latter implies that the γ-modification will become equivalent to the unmodified Newton–Raphson method if the iteration process approaches the actual solution of the problem. Fig. 1(b) illustrates the iteration procedure of the γ-modification for the example discussed above, in which $\kappa E_0/P_0 = 0.2$ and $D^{\text{ext}} = P_0$. The numerical parameters are taken to be $M = L = 0.3$. In contrast to the unmodified Newton–Raphson method, convergence is achieved. However, a disadvantage of the γ-modification is that the rate of convergence is relatively low as long as the criterion $d^{(k)} \ll L$ is not met.

2.3. D-modification of the Newton–Raphson method

The so-called "D-modification" is based upon the idea of directly inverting the relationship $D = D^{\text{mat}}(E, P^{\text{r,ref}})$ with respect to D and E within the "local material routines". In the following, the resulting inverse function is denoted by $E^{\text{mat}}(D, P^{\text{r,ref}})$. Now, the quantities $D^{(k),\text{int}}$ and $\kappa^{(k),\text{int}}$ in Eq. (2) are determined by

$$D^{(k),\text{int}} = \begin{cases} D^{\text{mat}}\left(E^{(0),\text{ext}}, P^{\text{r,ref}}\right) & \text{if } k = 0 \\ D^{\text{ext}} + \Delta D^{(k),\text{a}} & \text{if } k > 0, \end{cases} \tag{11}$$

$$\kappa^{(k),\text{int}} = \begin{cases} \kappa^{\text{mat}}\left(E^{(0),\text{ext}}, P^{\text{r,ref}}\right) & \text{if } k = 0 \\ \kappa^{\text{mat}}\left[E^{\text{mat}}\left(D^{\text{ext}}, P^{\text{r,ref}}\right), P^{\text{r,ref}}\right] & \text{if } k > 0, \end{cases} \tag{12}$$

where an "auxiliary electric displacement"

$$\Delta D^{(k),\text{a}} = \kappa^{(\text{k}),\text{int}} \cdot \left[E^{(k),\text{ext}} - E^{\text{mat}}\left(D^{\text{ext}}, P^{\text{r,ref}}\right)\right] \tag{13}$$

is introduced. The latter is necessary due to the fact that the return mapping is done at fixed electric displacement for the D-modification (and not at fixed electric field as for the unmodified Newton–Raphson method and the γ-modification). This leads to a difference between the electric field $E^{(k),\text{ext}}$ of the global iteration and the "material electric field" $E^{\text{mat}}\left(D^{\text{ext}}, P^{\text{r,ref}}\right)$, which has to be corrected. Note, that the initial iteration step of the D-modification is identical to the unmodified Newton–Raphson method. By inserting (11) and (12) into the "global" iteration rule (2) it can be easily verified that $E^{(k+1),\text{ext}} = E^{\text{mat}}(D^{\text{ext}}, P^{\text{r,ref}})$ for $k > 0$. This fact is illustrated in Fig. 1(c). As already stated, the result $E^{(1),\text{ext}}$ of the initial iteration step is the same as for the unmodified Newton–Raphson method. However, in contrast to the unmodified Newton–Raphson method, the tangent to the curve D^{mat} is now constructed in the point corresponding to the loading D^{ext}. Since this loading is assumed to be constant here, the iteration converges after the second iteration step and therefore $E^{(2),\text{ext}}$ is already the converged solution.

3. Generalisation to the multi-axial, fully coupled, ferroelectroelastic case

In this part of the paper, we discuss the generalisation of the unmodified Newton–Raphson method, the γ-modification and the D-modification to the fully coupled, ferroelectroelastic case. Furthermore, the restriction to homogeneous field distributions is dropped. Consequently, it is no longer sufficient to consider only a single material point. Rather, the strain tensor $\varepsilon_{ij}^{(k),\text{ext}}$ and the electric field vector $E_i^{(k),\text{ext}}$ are computed from the global finite element solution for each integration point of the finite elements after each equilibrium iteration step (denoted by k) of a load step. These quantities are passed to the "local material routines". As illustrated in Fig. 2, the task of the "local material routines" is to calculate the "internal" mechanical stress tensor $\sigma_{ij}^{(k),\text{int}}$, the "internal" electric displacement vector $D_i^{(k),\text{int}}$, the "internal" mechanical stiffness tensor at constant electric field $C_{ijmn}^{(k),E,\text{int}}$, the "internal" piezoelectric coupling tensor at constant strain $e_{mij}^{(k),\varepsilon,\text{int}}$, the "internal" piezoelectric coupling tensor at constant electric field $e_{imn}^{(k),E,\text{int}}$ and the "internal" permittivity tensor at constant strain $\kappa_{im}^{(k),\varepsilon,\text{int}}$ for each integration point. As in the electromechanically uncoupled, purely ferroelectric, homogeneous case discussed above, these quantities have to be chosen suitably to allow for convergence of the iteration to a valid solution. A further task of the "local material routines" is to compute the current remanent strain tensor $\varepsilon_{ij}^{\text{r},(k)}$ and the current remanent polarisation vector $P_i^{\text{r},(k)}$ after each equilibrium iteration step. After convergence of the global iteration scheme, the current material state becomes the reference state $\varepsilon_{ij}^{\text{r,ref}}$, $P_i^{\text{r,ref}}$ for the next load step at each integration point.

We define the "loads" which each material point (or integration point) has to carry after the $(k+1)$th equilibrium iteration step by

$$\begin{aligned} \sigma_{ij}^{(k+1),\text{ext}} &= \sigma_{ij}^{(k),\text{int}} + C_{ijmn}^{(k),E,\text{int}}\left(\varepsilon_{mn}^{(k+1),\text{ext}} - \varepsilon_{mn}^{(k),\text{ext}}\right) \\ &\quad - e_{mij}^{(k),\varepsilon,\text{int}}\left(E_m^{(k+1),\text{ext}} - E_m^{(k),\text{ext}}\right), \\ D_i^{(k+1),\text{ext}} &= D_i^{(k),\text{int}} + e_{imn}^{(k),E,\text{int}}\left(\varepsilon_{mn}^{(k+1),\text{ext}} - \varepsilon_{mn}^{(k),\text{ext}}\right) \\ &\quad + \kappa_{im}^{(k),\varepsilon,\text{int}}\left(E_m^{(k+1),\text{ext}} - E_m^{(k),\text{ext}}\right). \end{aligned} \tag{14}$$

Note here, that $e_{mij}^{(k),\varepsilon,\text{int}}$ is defined as usual with respect to the negative electric field. The electric fields are the negative gradient of the scalar potential, i.e. $E_i = -\phi_{,i}$. Since the scalar potential ϕ is a nodal degree of freedom, this choice leads to symmetric global finite element system matrices if the conditions

$$\begin{aligned} C_{ijmn}^{(k),E,\text{int}} &= C_{mnij}^{(k),E,\text{int}}, \\ e_{mij}^{(k),\varepsilon,\text{int}} &= e_{mij}^{(k),E,\text{int}}, \\ \kappa_{im}^{(k),\varepsilon,\text{int}} &= \kappa_{mi}^{(k),\varepsilon,\text{int}} \end{aligned} \tag{15}$$

are met. Additionally, permutability within the index pairs of $C_{ijmn}^{(k),E,\text{int}}$ and permutability of the last both indices of $e_{mij}^{(k),\varepsilon,\text{int}}$ and $e_{imn}^{(k),E,\text{int}}$ is required. This can be always achieved due to the symmetry of the strain tensor and the mechanical stress tensor.

It is possible to write (14) in a similar form as (2) by solving for $\varepsilon_{ij}^{(k+1),\text{ext}}$ and $E_i^{(k+1),\text{ext}}$. Thus, on the local level, the iteration process may be interpreted analogously as for homogeneous field distributions. But now, the "loads" $\sigma_{ij}^{(k),\text{ext}}$ and $D_i^{(k),\text{ext}}$ are no longer necessarily constant throughout the iteration. However, they converge as the global finite element iteration converges to a solution.

In the multi-axial, fully coupled, ferroelectroelastic case, the material behaviour is described by the functions $\sigma_{ij}^{\text{mat}}(\varepsilon_{rs}, E_r, \varepsilon_{rs}^{\text{r,ref}}, P_r^{\text{r,ref}})$ and $D_i^{\text{mat}}(\varepsilon_{rs}, E_r, \varepsilon_{rs}^{\text{r,ref}}, P_r^{\text{r,ref}})$, which assign the "material mechanical stresses" and the "material electric displacements" based on the total strains ε_{rs} and the electric fields E_r at the end of a load step. The parameters $\varepsilon_{rs}^{\text{r,ref}}$ and $P_r^{\text{r,ref}}$ characterise the materials reference state at the beginning of the load step. For clarity, these parameters are omitted in the following. The consistent tangent stiffness tensor at constant electric field $C_{ijmn}^{E,\text{mat}}$, the consistent tangent piezoelectric coupling tensor at constant mechanical strain $e_{mij}^{\varepsilon,\text{mat}}$, the consistent tangent piezoelectric coupling tensor

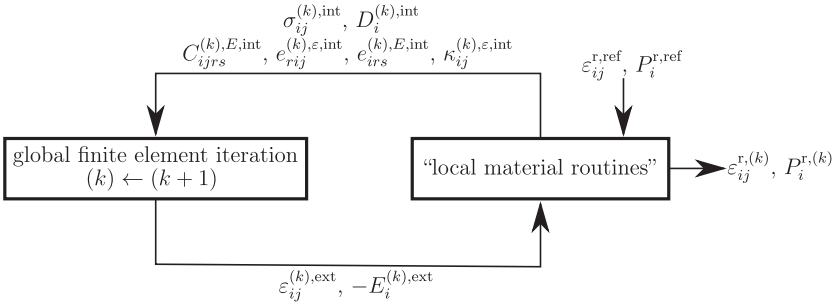

Fig. 2. Interaction between global finite element iteration and "local material routines".

at constant electric field $e_{imn}^{E,\mathrm{mat}}$ and the consistent tangent permittivity at constant strain $\kappa_{im}^{\varepsilon,\mathrm{mat}}$ are defined as

$$\begin{aligned} C_{ijmn}^{E,\mathrm{mat}} &= \frac{\partial \sigma_{ij}^{\mathrm{mat}}}{\partial \varepsilon_{mn}}, \\ e_{mij}^{\varepsilon,\mathrm{mat}} &= -\frac{\partial \sigma_{ij}^{\mathrm{mat}}}{\partial E_m}, \\ e_{imn}^{E,\mathrm{mat}} &= \frac{\partial D_i^{\mathrm{mat}}}{\partial \varepsilon_{mn}}, \\ \kappa_{im}^{\varepsilon,\mathrm{mat}} &= \frac{\partial D_i^{\mathrm{mat}}}{\partial E_m}. \end{aligned} \tag{16}$$

In order to satisfy the symmetry conditions (15) in the following, a symmetrisation is applied:

$$\begin{aligned} C_{ijmn}^{E,\mathrm{mat,sym}} &= \frac{1}{2}\left(C_{ijmn}^{E,\mathrm{mat}} + C_{mnij}^{E,\mathrm{mat}}\right), \\ e_{mij}^{\varepsilon,\mathrm{mat,sym}} &= \frac{1}{2}\left(e_{mij}^{\varepsilon,\mathrm{mat}} + e_{mij}^{E,\mathrm{mat}}\right), \\ e_{imn}^{E,\mathrm{mat,sym}} &= \frac{1}{2}\left(e_{imn}^{\varepsilon,\mathrm{mat}} + e_{imn}^{E,\mathrm{mat}}\right), \\ \kappa_{im}^{\varepsilon,\mathrm{mat,sym}} &= \frac{1}{2}\left(\kappa_{im}^{\varepsilon,\mathrm{mat}} + \kappa_{mi}^{\varepsilon,\mathrm{mat}}\right). \end{aligned} \tag{17}$$

Note, that the use of the symmetrised quantities may reduce the rate of convergence of the global finite element iteration. However, we expect that this disadvantage is overcompensated by the higher efficiency of methods available for solving symmetric systems of equations.

3.1. Unmodified Newton–Raphson method

For the unmodified Newton–Raphson method, the "internal" quantities are determined by

$$\begin{aligned} \sigma_{ij}^{(k),\mathrm{int}} &= \sigma_{ij}^{\mathrm{mat}}\left(\varepsilon_{rs}^{(k),\mathrm{ext}}, E_r^{(k),\mathrm{ext}}\right), \\ D_i^{(k),\mathrm{int}} &= D_i^{\mathrm{mat}}\left(\varepsilon_{rs}^{(k),\mathrm{ext}}, E_r^{(k),\mathrm{ext}}\right), \\ C_{ijmn}^{(k),E,\mathrm{int}} &= C_{ijmn}^{E,\mathrm{mat,sym}}\left(\varepsilon_{rs}^{(k),\mathrm{ext}}, E_r^{(k),\mathrm{ext}}\right), \\ e_{mij}^{(k),\varepsilon,\mathrm{int}} &= e_{mij}^{\varepsilon,\mathrm{mat,sym}}\left(\varepsilon_{rs}^{(k),\mathrm{ext}}, E_r^{(k),\mathrm{ext}}\right), \\ e_{imn}^{(k),E,\mathrm{int}} &= e_{imn}^{E,\mathrm{mat,sym}}\left(\varepsilon_{rs}^{(k),\mathrm{ext}}, E_r^{(k),\mathrm{ext}}\right), \\ \kappa_{im}^{(k),\varepsilon,\mathrm{int}} &= \kappa_{im}^{\varepsilon,\mathrm{mat,sym}}\left(\varepsilon_{rs}^{(k),\mathrm{ext}}, E_r^{(k),\mathrm{ext}}\right). \end{aligned} \tag{18}$$

3.2. γ-Modification of the Newton–Raphson method

For the γ-modification, the "internal" quantities are determined by

$$\begin{aligned} \sigma_{ij}^{(k),\mathrm{int}} &= \sigma_{ij}^{(k),\mathrm{ext}} + \gamma^{(k)}\left[\sigma_{ij}^{\mathrm{mat}}\left(\varepsilon_{rs}^{(k),\mathrm{ext}}, E_r^{(k),\mathrm{ext}}\right) - \sigma_{ij}^{(k),\mathrm{ext}}\right] = \sigma_{ij}^{(k),\mathrm{ext}} + \gamma^{(k)} \cdot \Delta\sigma_{ij}^{(k)}, \\ D_i^{(k),\mathrm{int}} &= D_i^{(k),\mathrm{ext}} + \gamma^{(k)}\left[D_i^{\mathrm{mat}}\left(\varepsilon_{rs}^{(k),\mathrm{ext}}, E_r^{(k),\mathrm{ext}}\right) - D_i^{(k),\mathrm{ext}}\right] = D_i^{(k),\mathrm{ext}} + \gamma^{(k)} \cdot \Delta D_i^{(k)}, \\ C_{ijmn}^{(k),E,\mathrm{int}} &= C_{ijmn}^{E,\mathrm{mat,sym}}\left(\varepsilon_{rs}^{(k),\mathrm{ext}}, E_r^{(k),\mathrm{ext}}\right), \\ e_{mij}^{(k),\varepsilon,\mathrm{int}} &= e_{mij}^{\varepsilon,\mathrm{mat,sym}}\left(\varepsilon_{rs}^{(k),\mathrm{ext}}, E_r^{(k),\mathrm{ext}}\right), \\ e_{imn}^{(k),E,\mathrm{int}} &= e_{imn}^{E,\mathrm{mat,sym}}\left(\varepsilon_{rs}^{(k),\mathrm{ext}}, E_r^{(k),\mathrm{ext}}\right), \\ \kappa_{im}^{(k),\varepsilon,\mathrm{int}} &= \kappa_{im}^{\varepsilon,\mathrm{mat,sym}}\left(\varepsilon_{rs}^{(k),\mathrm{ext}}, E_r^{(k),\mathrm{ext}}\right). \end{aligned} \tag{19}$$

Here, $\sigma_{ij}^{(k),\mathrm{ext}}$ and $D_i^{(k),\mathrm{ext}}$ can be calculated from known quantities by using (14). We propose the relationship

$$\gamma^{(k)} = (1-M) \cdot \exp\left(-\frac{\sqrt{\Delta D_m^{(k)} \Delta D_m^{(k)}}}{P_0 L}\right) + M \tag{20}$$

as an extension of (10) for the computation of $\gamma^{(k)}$ in the electromechanically coupled, multi-axial case. Only the absolute value of the normalised electric displacement residual vector $\Delta D_m^{(k)}/P_0$ is utilised as a measure for the accuracy of the local solution after the kth equilibrium iteration step since the convergence problems arise from the electrical part of the problem. Thus, no scaling is necessary in purely mechanical situations.

3.3. D-modification of the Newton–Raphson method

For the D-modification, inversion of the relationship $D_i = D_i^{\mathrm{mat}}(\varepsilon_{rs}, E_r, \varepsilon_{rs}^{\mathrm{r,ref}}, P_r^{\mathrm{r,ref}})$ with respect to D_i and E_r is required. The resulting inverse function is denoted by $E_i^{\mathrm{mat}}(\varepsilon_{rs}, D_r, \varepsilon_{rs}^{\mathrm{r,ref}}, P_r^{\mathrm{r,ref}})$. This function corresponds to a return mapping at fixed strain and electric displacement. With the help of E_i^{mat}, the "internal" quantities are determined by

$$\begin{aligned} \sigma_{ij}^{(k),\mathrm{int}} &= \sigma_{ij}^{\mathrm{mat}}\left[\varepsilon_{rs}^{(k),\mathrm{ext}}, E_r^{\mathrm{mat}}\left(\varepsilon_{pq}^{(k),\mathrm{ext}}, D_p^{(k),\mathrm{ext}}\right)\right] + \Delta\sigma_{ij}^{(k),\mathrm{a}}, \\ D_i^{(k),\mathrm{int}} &= D_i^{(k),\mathrm{ext}} + \Delta D_i^{(k),\mathrm{a}}, \\ C_{ijmn}^{(k),E,\mathrm{int}} &= C_{ijmn}^{E,\mathrm{mat,sym}}\left[\varepsilon_{rs}^{(k),\mathrm{ext}}, E_r^{\mathrm{mat}}\left(\varepsilon_{pq}^{(k),\mathrm{ext}}, D_p^{(k),\mathrm{ext}}\right)\right], \\ e_{mij}^{(k),\varepsilon,\mathrm{int}} &= e_{mij}^{\varepsilon,\mathrm{mat,sym}}\left[\varepsilon_{rs}^{(k),\mathrm{ext}}, E_r^{\mathrm{mat}}\left(\varepsilon_{pq}^{(k),\mathrm{ext}}, D_p^{(k),\mathrm{ext}}\right)\right], \\ e_{imn}^{(k),E,\mathrm{int}} &= e_{imn}^{E,\mathrm{mat,sym}}\left[\varepsilon_{rs}^{(k),\mathrm{ext}}, E_r^{\mathrm{mat}}\left(\varepsilon_{pq}^{(k),\mathrm{ext}}, D_p^{(k),\mathrm{ext}}\right)\right], \\ \kappa_{im}^{(k),\varepsilon,\mathrm{int}} &= \kappa_{im}^{\varepsilon,\mathrm{mat,sym}}\left[\varepsilon_{rs}^{(k),\mathrm{ext}}, E_r^{\mathrm{mat}}\left(\varepsilon_{pq}^{(k),\mathrm{ext}}, D_p^{(k),\mathrm{ext}}\right)\right] \end{aligned} \tag{21}$$

for $k \geqslant 1$, where the "auxiliary mechanical stresses" $\Delta\sigma_{ij}^{(k),\mathrm{a}}$ and the "auxiliary electric displacements" $\Delta D_i^{(k),\mathrm{a}}$ are:

$$\begin{aligned} \Delta\sigma_{ij}^{(k),\mathrm{a}} &= -e_{mij}^{(k),\varepsilon,\mathrm{int}} \cdot \left[E_m^{(k),\mathrm{ext}} - E_m^{\mathrm{mat}}\left(\varepsilon_{rs}^{(k),\mathrm{ext}}, D_r^{(k),\mathrm{ext}}\right)\right], \\ \Delta D_i^{(k),\mathrm{a}} &= \kappa_{im}^{(k),\varepsilon,\mathrm{int}} \cdot \left[E_m^{(k),\mathrm{ext}} - E_m^{\mathrm{mat}}\left(\varepsilon_{rs}^{(k),\mathrm{ext}}, D_r^{(k),\mathrm{ext}}\right)\right]. \end{aligned} \tag{22}$$

As for the γ-modification, $D_i^{(k),\mathrm{ext}}$ follows from the second equation in (14). Both modifications use the relations (18) of the unmodi-

fied Newton–Raphson method before the first equilibrium iteration ($k = 0$). By inserting (21) and (22) into (14) it can be verified that the *D*-modification will yield a converged result after the second equilibrium iteration step if fixed strains $\varepsilon_{ij}^{(k),\text{ext}}$ and fixed electric displacements $D_i^{(k),\text{ext}}$ are prescribed. In contrast, the unmodified Newton–Raphson method and the γ-modification converge instantaneously in cases of fixed strains $\varepsilon_{ij}^{(k),\text{ext}}$ and fixed electric fields $E_i^{(k),\text{ext}}$. Thus, as stated above, the *D*-modification switches the roles of electric fields and electric displacements locally without changing the global iteration scheme.

In the following, we shall show that the *D*-modification and the vector potential formulation combined with the unmodified Newton–Raphson method yield a virtually identical iteration scheme (we emphasise the term "virtually", since differences between both methods arise due to the finite element discretisation as described below). In this context, it is important to note that the unmodified Newton–Raphson method generally consists of a series of linearisations. This procedure is described for the vector potential formulation below. Let $\varepsilon_{kl}^{(k),\text{ext}}$ be the mechanical strain solution derived from the displacement field $u_k^{(k)}$ after the kth equilibrium iteration step of a non-linear finite element calculation and let $D_k^{(k),\text{ext}}$ be the corresponding electric displacement solution derived from the vector potential field $\psi_k^{(k)}$. Then, the next solution for the displacement field $u_k^{(k+1)}$ and the vector potential field $\psi_k^{(k+1)}$ (and therefore the next solution for the mechanical strain field $\varepsilon_{kl}^{(k+1),\text{ext}}$ and the electric displacement field $D_k^{(k+1),\text{ext}}$) is obtained by linearising the material behaviour around $\left\{\left[\varepsilon_{kl}^{(k),\text{ext}}, D_k^{(k),\text{ext}}\right]; \left[\sigma_{kl}^{\text{mat}}(\varepsilon_{ij}^{(k),\text{ext}}, D_i^{(k),\text{ext}}), E_k^{\text{mat}}(\varepsilon_{ij}^{(k),\text{ext}}, D_i^{(k),\text{ext}})\right]\right\}$ at the integration points of the finite elements and calculating a new solution based on the given boundary conditions. This procedure is repeated until convergence is achieved. The *D*-modification applies a similar iteration algorithm by linearising around the same point. Thereby, the difference $E_k^{(k),\text{ext}} - E_k^{\text{mat}}(\varepsilon_{ij}^{(k),\text{ext}}, D_i^{(k),\text{ext}})$, which results from the fact that the scalar potential is the nodal degree of freedom, is compensated by introducing the auxiliary mechanical stresses and auxiliary electric displacements. Note, that this has no influence on the point of linearisation. Consequently, the only major difference between the vector potential formulation combined with the unmodified Newton–Raphson method and the *D*-modification is that, for the latter, the electric displacements $D_k^{(k),\text{ext}}$ at an integration point can not be directly computed from the nodal quantities. Rather, these electric displacements are obtained from (14) by using the linearised material behaviour of the previous iteration step. However, it can be shown that the resulting electric displacements are consistent with the nodal charges. Additional differences between the vector potential formulation combined with the unmodified Newton–Raphson method and the *D*-modification can arise from the fact that different quantities are discretised by the shape functions. This leads to a different accessible solution space, which may lead to a better convergence behaviour of one or the other method, depending on the exact problem under consideration. Due to the described similarities, it is expected that the *D*-modification shows a comparable behaviour as the vector potential formulation combined with the unmodified Newton–Raphson method. However, the outstanding advantages of the *D*-modification are that it does not require gauging, allows for a simple implementation of common boundary conditions and saves two degrees of freedom per finite element node.

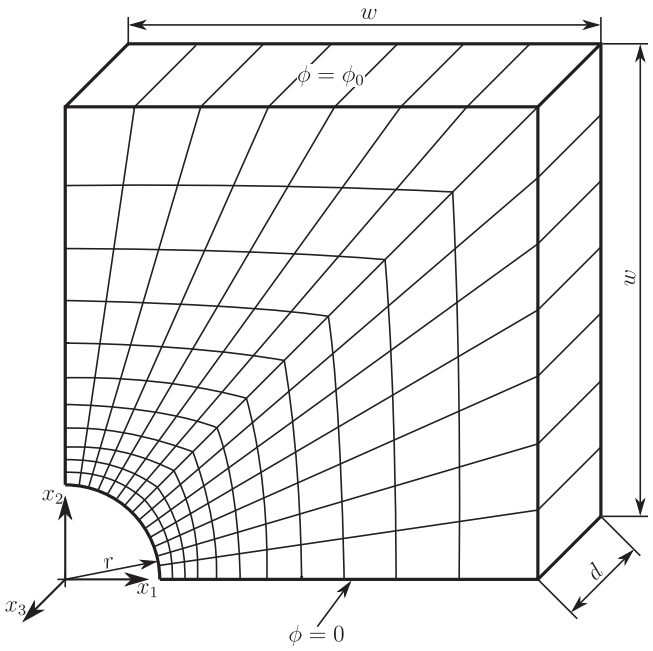

Fig. 3. Finite element model of hexahedron with hole.

4. Numerical example

4.1. Geometry and boundary conditions

In order to demonstrate the capabilities of the methods described above, the poling of a hexahedron containing a centered cylindrical hole is simulated with the finite element method, where the geometry is taken from Semenov et al. (2009) (edge length $2w = 20$ mm, thickness $2d = 6$ mm, diameter $2r = 4$ mm). Due to the symmetries/anti-symmetries in geometry and boundary conditions, only one eighth of the hexahedron is modelled. Fig. 3 shows the resulting finite element model. The mesh is composed of 154 20-noded elements with quadratic shape functions and 14 integration points. Only one element is used for discretisation in thickness direction.

In the symmetry planes $x_1 = 0$ and $x_2 = 0$ the normal component of the displacement vector is set to zero. Furthermore, the displacement in x_3-direction is prohibited at all nodes. This corresponds to a plane strain state. As shown in Fig. 3, the scalar potential $\phi = \phi_0$ is prescribed on the upper face of the hexahedron at $x_2 = w$. In the plane $x_2 = 0$ the scalar potential is constrained to $\phi = 0$, which incorporates an anti-symmetric distribution of electric fields and electric displacements. Vanishing tractions and vanishing free surface charges are assumed for all remaining boundary conditions. In order to derive the electrical boundary conditions from the jump conditions at the boundaries $x_1 = w$ and $x_3 = -d$, the domain external to the body is taken to be approximately free of electric displacements. This leads to $D_1 = 0$ at the surface $x_1 = w$ and $D_3 = 0$ at the surface $x_3 = -d$. The boundary conditions assumed here result in a plane electrical and mechanical state. Nevertheless, three-dimensional finite elements are used since plane elements have not been implemented yet.

Table 1
Material parameters for PIC151, fitted to experimental data of Zhou (2003).

Parameter	Symbol	Value	Unit
Young's modulus	Y	120	GPa
Poisson's ratio	ν	0.31	–
Dielectric permittivity	κ	2.2×10^{-8}	F/m
Piezoelectric constants	d_{31}	-1.7×10^{-10}	m/V
	d_{33}	4.0×10^{-10}	m/V
	d_{15}	4.6×10^{-10}	m/V
Saturation polarisation	P_0	0.415	C/m^2
Compressive saturation strain	ε_0	0.0032	–
Coercive electric field	E_0	0.92	MV/m
Coercive mechanical stress	σ_0	35	MPa
Hardening parameters	H_0^e	350000	m/F
	m^e	2.0	–
	H_0^σ	350	MPa
	m^c	2.0	–
	m^t	2.0	–
	H_0^π	0	m/F
Switching surface shape factor	β	2.0	–

4.2. Material

The fully coupled, multi-axial, phenomenological, macroscopic material model presented by Landis (2002a) is utilised to describe the material behaviour. We use a return mapping algorithm (Semenov et al., 2009) for the numerical integration of the constitutive equations, where the evolution equations for the remanent strains and polarisations are discretised with the backward Euler method. The material parameters shown in Table 1 are chosen to fit the bipolar hysteresis experiments and the mechanical compression experiments conducted by Zhou (2003) for the soft lead circonate titanate (PZT) ceramic PIC151. Note, that these material parameters have not been verified for experiments under combined electrical and mechanical loading. Therefore, they can not be expected to give a complete representation of the material behaviour of PIC151. Rather, the material parameters should be seen as a basis for testing the numerical methods described above.

Table 2
Number of load increments and equilibrium iterations for different iteration methods/modifications and parameters, Tolerance $\epsilon = 1 \times 10^{-6}$.

Method/modification	Load increments	Equilibrium iterations Σ
Unmodified Newton–Raphson	>200	–
γ ($M = 0.03, L = 0.11$)	1	37
γ ($M = 0.3, L = 0.11$)	1	12
D	1	9
Vector potential	1	9

4.3. Results

In this section, results for an increase of the prescribed normalised potential from zero to $|\phi_0|/(E_0 w) = 1$ are presented. If there was no hole in the hexahedron, the resulting applied potential of $|\phi_0| = 9.2$ kV would lead to a uniform electric field equal to the coercive electric field E_0. Note, that initially the material is free of remanent strains and polarisations everywhere.

The calculation is done with the commercially available finite element software ANSYS, where a user defined finite element is used along with appropriate material routines. A tolerance of $\epsilon = 1 \times 10^{-6}$ about the typical values of the nodal degrees of freedom and the nodal forces/charges is used as convergence criterion, where the convergence check is performed at each node and degree of freedom individually (infinity norm). The loading ϕ_0 is split up into as many equally spaced load increments as are required to achieve convergence. Thereby, a single load increment is considered to be not converged if a number of 50 equilibrium iterations is exceeded without satisfying the convergence criteria or the return mapping procedure fails.

The number of required load increments and equilibrium iterations is shown in Table 2 for the different iteration methods/modifications. Even with 200 load increments, it is not possible to achieve convergence with the unmodified Newton–Raphson method. This is primarily due to oscillating solutions during the equilibrium iteration process as described above. In contrast, the γ-modification requires only 1 load increment for convergence. However, it can be seen from the results in Table 2 that the number of equilibrium iterations strongly depends on the numerical parameters M and L chosen. Note, that the probability of non-convergence increases as the numerical parameters are modified in a way that the γ-modification approaches the unmodified Newton–Raphson method (even though the number of required equilibrium iterations decreases in Table 2). The D-modification converges within a single load increment and only 9 equilibrium iterations. For comparison, a result obtained with the vector potential formulation is also included in Table 2. This calculation was performed with the finite element code PANTOCRATOR (Semenov, 2003), where the same mesh as for the scalar potential formulation was used. As for the D-modification, one load increment and 9 equilibrium iterations are required for convergence. This result supports the assertion that the scalar potential formulation combined with the D-modification shows a convergence behaviour comparable to the vector potential formulation.

It is noted that the number of required load increments is much higher for the D-modification than for the vector potential formulation if 8-noded finite elements with 8 integration points are used. We believe that this is due to oscillations occuring in the electric

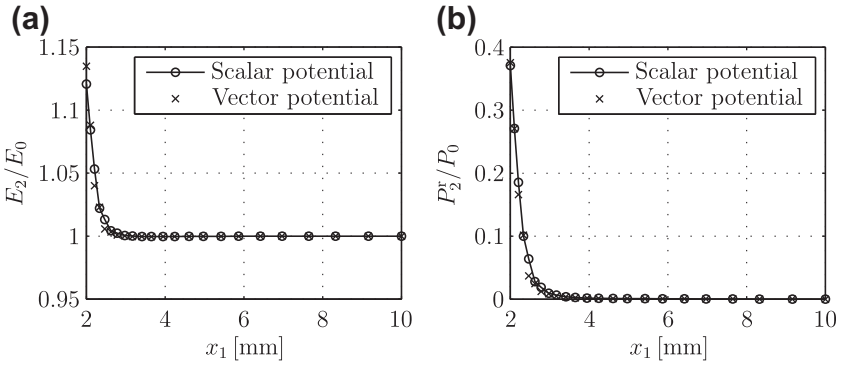

Fig. 4. Finite element results for $|\phi_0|/(E_0 d) = 1$ in the symmetry/anti-symmetry plane $x_2 = 0$ along a path in x_1-direction: (a) Normalised electric field E_2/E_0 and (b) Normalised remanent polarisation P_2^r/P_0.

field solution, which are caused by the linear shape functions utilised for the discretisation of the scalar potential. These oscillations increase within the iteration process, leading to divergence of the solution. Probably, this unstable numerical behaviour is associated with the strongly varying tangent permittivity. The effect described was found to be highly dependent on the finite element model under consideration, where the mesh (particularly the orientation of the elements with respect to the electric field) seems to play a crucial role. Therefore, it is likely that similar problems can be observed for the vector potential formulation for other examples. Thus, we generally do not recommend the usage of finite elements with linear shape functions.

The field solutions obtained with the scalar potential formulation and the vector potential formulation are compared to each other in Fig. 4. The results are plotted along a path in x_1-direction in the symmetry/anti-symmetry plane $x_2 = 0$. For the scalar potential formulation, the curves shown are the same for D-modification and γ-modification within the accuracy imposed by the convergence criteria. Due to the boundary conditions, there is no dependency on the co-ordinate x_3. Fig. 4(a) depicts the normalised electric field E_2/E_0 and Fig. 4(b) shows the normalised remanent polarisation P_2^r/P_0. The agreement between scalar potential formulation and vector potential formulation is reasonable even though the mesh is coarse. Note, that the electric field is elevated over its nominal value only very close to the hole and the ratio between maximum electric field and nominal electric field is relatively low ($E_{2,\max}/E_0 \approx 1.13$). Moreover, as can be seen in Fig. 4(b), the remanent polarisation level stays far away from saturation. However, the range of small remanent polarisations and therefore electric fields close to the coercive electric field is most problematical for finite element computations of ferroelectroelastic ceramics based on the scalar potential formulation. If a higher loading than $|\phi_0|/(E_0 d) = 1$ is applied, the convergence behaviour becomes better due to the material saturation properties. Consequently, for a sufficiently high level of loading, even the unmodified Newton–Raphson method converges as discussed above.

The example demonstrates only the capabilities of the D-modification and the γ-modification for the poling of a specimen. We have tested further load cases including higher applied potentials $|\phi_0|$, reversal of the poling direction by changing the sign of the applied potential ϕ_0 and mechanical depolarisation by applying pressure on the upper face at $x_2 = w$ after removal of ϕ_0. No significant convergence difficulties are experienced in these examples with D-modification and γ-modification. However, relatively small load increments are required for the mechanical depolarisation once the applied pressure exceeds the coercive stress σ_0. This behaviour is also found if pressure of this level is applied to the unpoled configuration. It is therefore concluded that this effect results from the shape of the purely ferroelastic material hysteresis. Note, that for such purely mechanical load cases all methods discussed here, including the vector potential formulation, yield identical results given that no initial remanent polarisation is present.

5. Concluding remarks

In the present paper, methods to improve the convergence behaviour of non-linear finite element computations with the scalar potential formulation utilised are discussed. Starting from the simple purely ferroelectric case with homogeneous field distributions and loading in a fixed direction, the methods have been extended to the multi-axial, fully electromechanically coupled, ferroelectroelastic case. A numerical example has shown the convergence difficulties of the unmodified Newton–Raphson method. The two modifications of the Newton–Raphson method proposed to reduce or eliminate these problems, namely the γ-modification and the D-modification, were both succesfully tested in the numerical example. A disadvantage of the γ-modification is the requirement of choosing the numerical parameters L and M. In this context, it is desirable to develop methods which assign the value of $\gamma^{(k)}$ adaptively, based on the convergence behaviour in previous equilibrium iteration steps. The attractiveness of the D-modification is that it does not require such numerical parameters and shows convergence properties similar to the vector potential formulation combined with the unmodified Newton–Raphson method.

Acknowledgements

The authors of the present paper are indebted to A.S. Semenov for providing the finite element results of the vector potential formulation. Support of the Deutsche Forschungsgemeinschaft (DFG) under Grants BA 1411/12-2 and BA 1411/13-2 is gratefully acknowledged.

References

Allik, H., Hughes, T., 1970. Finite element method for piezoelectric vibration. International Journal for Numerical Methods in Engineering 2, 151–157.

Cocks, A., McMeeking, R., 1999. A phenomenological constitutive law for the behaviour of ferroelectric ceramics. Ferroelectrics 228, 219–228.

Ghandi, K., Hagood, N., 1997. A hybrid finite element model for phase transitions in nonlinear electro-mechanically coupled material. In: Varadan, V., Chandra, J. (Eds.), Smart Structures and Materials: Mathematics and Control in Smart Structures, pp. 97–112.

Huber, J., Fleck, N., Landis, C., McMeeking, R., 1999. A constitutive model for ferroelectric polycrystals. Journal of the Mechanics and Physics of Solids 47, 1663–1697.

Huo, Y., Jiang, Q., 1997. Modeling of domain switching in polycrystalline ferroelectric ceramics. Smart Materials and Structures 6, 441–447.

Hwang, S., Lynch, C., McMeeking, R., 1995. Ferroelectric/ferroelastic interactions and a polarization switching model. Acta Metallurgica et Materialia 42, 2073–2084.

Kamlah, M., Wang, Z., 2003. A thermodynamically and microscopically motivated constitutive model for piezoceramics. Computational Materials Science 28, 409–418.

Klinkel, S., 2006. A phenomenological constitutive model for ferroelastic and ferroelectric hysteresis effects in ferroelectric ceramics. International Journal of Solids and Structures 43, 7197–7222.

Landis, C., 2002a. Fully coupled, multi-axial, symmetric constitutive laws for polycrystalline ferroelectric ceramics. Journal of the Mechanics and Physics of Solids 50, 127–152.

Landis, C., 2002b. A new finite-element formulation for electromechanical boundary value problems. International Journal for Numerical Methods in Engineering 55, 613–628.

Mehling, V., Tsakmakis, C., Gross, D., 2007. Phenomenological model for the macroscopical material behavior of ferroelectric ceramics. Journal of the Mechanics and Physics of Solids 55, 2106–2141.

Neumeister, P., Balke, H., 2011. Micromechanical modelling of remanent properties of morphotropic PZT. Journal of the Mechanics and Physics of Solids 59, 1794–1807.

Pathak, A., McMeeking, R., 2008. Three-dimensional finite element simulations of ferroelectric polycrystals under electrical and mechanical loading. Journal of the Mechanics and Physics of Solids 56, 663–683.

Roth, S., Neumeister, P., Semenov, A., Balke, H., 2009. Finite element simulation of the non-remanent straining ferroelectric material behaviour based on the electrostatic scalar potential – convergence and stability. In: Kuna, M., Ricoeur, A. (Eds.), Proceedings of the IUTAM Symposium on Multiscale Modelling of Fatigue, Damage and Fracture in Smart Materials, pp. 55–66.

Schwaab, H., Grünbichler, H., Supancic, P., Kamlah, M., 2012. Macroscopical nonlinear material model for ferroelectric materials inside a hybrid finite element formulation. International Journal of Solids and Structures 49, 457–469.

Semenov, A., 2003. PANTOCRATOR – the finite element program specialized on the nonlinear problem solution. In: Proceedings of the Fifth International Conference on Scientific and Engineering Problems of Predicting the Reliability and Service Life of Structures and Methods of their Solution, pp. 466–480.

Semenov, A., Kessler, H., Liskowsky, A., Balke, H., 2006. On a vector potential formulation for 3D electromechanical finite element analysis. Communications in Numerical Methods in Engineering 22, 357–375.

Semenov, A., Liskowsky, A., Balke, H., 2009. Return mapping algorithms and consistent tangent operators in ferroelectroelasticity. International Journal for Numerical Methods in Engineering 81, 1298–1340.

Zhou, D., 2003. Experimental Investigation of Non-linear Constitutive Behavior of PZT Piezoceramics. Dissertation. Forschungszentrum Karlsruhe.